Advances in interferometric techniques for the analysis of the three-dimensional flow in a lid-driven cylindrical cavity

Ana Mª López[1], Julia Lobera[1], Nieves Andrés[1], Mª Pilar Arroyo[1], Virginia Palero[1*], Irene Sancho[2], Antón Vernet[2], Jordi Pallarés[2]

[1]Instituto de Investigación en Ingeniería de Aragón (I3A), Universidad de Zaragoza, Zaragoza, Spain.
[2]Departamento de Ingeniería Mecánica, Universitat Rovira i Virgili, Campus Sescelades, Tarragona, Spain.
Correspondent author: palero@unizar.es; +34-976762691

Keywords: Digital in-line holography; 3D flow measurement; rotating flow; particle tracking; flow visualization

ABSTRACT

In this work a qualitative and quantitative characterization of the three-dimensional flow in a lid-driven cylindrical cavity with different optical techniques is presented. Mach-Zehnder interferometry and photographic techniques have been used for a qualitative description of some flow features. However, the real challenge is to obtain quantitative measurements, as the cavity dimensions and geometry prevent the application of 3D digital techniques for measuring the flow velocity in the whole cavity with enough spatial resolution. Digital in-line Holography was applied to the measure of the vortex-breakdown bubble that appears near the cavity bottom at Re=2000. A 22x22x80mm^3 volume was recorded, its longest dimension parallel to the camera optical axis. This large volume in a liquid fluid combined with a high particle density forces us to develop new analysis strategies.

Holograms have been analyzed using a new method, called Adaptive Cross Correlation with Tracking From Beginning, which includes the use of the reconstructed complex amplitude for particle localization. Particle tracking is based on the three-dimensional cross-correlation of three-dimensional interrogation windows. The particle set defined in the first hologram is always used to find the particle position in subsequent holograms. This method provides an accurate 3D velocity map and the vortex-breakdown bubble spatial structure. Experimental and numerical data show a very good agreement. A new criterion for determining the accuracy in the particle position along the optical axis is introduced, achieving a spatial resolution of 0.1 mm. This tracking method can be applied not only to laminar flows but also to turbulent flows.

---

1. Introduction

The analysis of confined flows is of interest for basic research and for many technological applications. The flow generated in lid driven cavities has attracted the attention of many researches, as the problem configuration and its geometry are simple and physically feasible. In contrast, the flow exhibits a relatively complex behavior, especially as the Reynolds number (or for example, the velocity of the lid) is progressively increased (Shankar and Deshpande, 2000). Flow features such as corner and longitudinal vortices, three-dimensionality and a progressive transition to turbulence can be analyzed in this simple flow configuration.

The flow in a cylindrical cavity generated by a rotating lid has been extensively studied, numerically and experimentally, in the last 30 years (Escudier 1984; Lopez 1990; Brown and Lopez 1990, Lopez and Perry 1992;

Gelfgat et al. 1996; Lucca-Negro and O'Doherty 2001; Sotiropoulos and Ventikos 2001; Brøns et al. 2007; Spohn et al. 2008; Sancho et al. 2016) and the flow field in the laminar regime has been characterized (Escudier 1984; Spohn et al. 2008; Cabeza et al. 2010). At low rotational Reynolds numbers ($Re=\omega R^2/\nu$), based on the maximum linear velocity of the lid (ωR) and the kinematic viscosity of the fluid (ν), the flow exhibits axisymmetric steady vortex breakdown phenomena. As Re is increased, the flow becomes unsteady and it shows different modes or non-axisymmetric flow structures, with characteristic wavelengths, distributed along the azimuthal direction (Sørensen et al. 2006).

The objective of this work is to apply optical, non-intrusive, laser techniques to study different features of a laminar, confined flow in a cylindrical cavity with a rotating end-wall. These techniques will provide with both qualitative and quantitative information. Particle Image Velocity (PIV) and Planar Laser Induced Fluorescence (PLIF) were applied in a previous work (Sancho et al. 2016) to measure the velocity and concentration fields in such a system. In these experiments when the flow was steady an acid solution was injected at low velocity to the initially basic solution inside the cavity. The fluorescent dye was added to the injected acid solution that was also seeded with particles for PIV measurements. In this case, the seeding particles were functionalized with Rhodamine, which enables to separate the particle scattered light from the fluorescent intensity. Changes of the fluorescence intensity, produced by the changes in the pH inside the cavity, allowed obtaining quantitative information about the local concentration evolution. However, the use of fluorescent substances, which may be toxic, requires a careful handling and an environment-safe disposal.

Although we will not produce any chemical reaction, we can visualize some of the spatial structures obtained in Sancho et al. (2016), without the use of fluorescence. The visualization will be done by applying Mach-Zehnder interferometry (Vest, 1979) or PIV (Raffel et al. 1998-2007) when liquids with different characteristics are injected to the cavity. The first technique allows visualizing the three-dimensional (3D) flow structures obtained when combining two liquids with different refractive index. With PIV and injecting a highly seeded liquid it is possible to directly visualize the particle streamlines in a fluid plane.

A quantitative 3D measurement of the three-component (3C) velocity field is needed in order to completely characterize the flow. Several techniques have been developed to measure the 3D-3C velocity field in a fluid, as tomographic PIV (Elsinga et al. 2006) or Digital Holography (Schnars and Jüptner 2005; Arroyo and Hinsch 2008; Katz and Sheng 2010) among others. In tomographic PIV the light scattered by the particles in a volume is recorded simultaneously from several viewing directions, which implies the use of several cameras and a complicated calibration procedure. Besides, its application in confined and in liquid flows is seriously limited. Digital Holography is a full 3D-3C technique that allows the recording of a fluid volume with only one camera. This is achieved by making interfere in a digital sensor the light scattered by the object with a reference beam. Therefore, both the amplitude and the phase of the object wave are captured. Two are the most used configurations: the in-line and the off-axis holography. Although some efforts have been done to extend the application of digital off-axis holography to the measurement of flow velocity (Lobera et al. 2003; Sheng et al. 2003, Palero et al. 2010) the simplicity of the in-line configuration prevails (Pan and Meng 2003; Palero et al. 2013) and it is applied in most cases.

Digital in-line holography (DIH from now on) presents two disadvantages. The low spatial resolution of the digital cameras prevents the recording of high spatial frequencies and forces the use of small angles between the object and the reference beam. As a consequence the virtual and real images are not fully separated when the hologram is reconstructed. To obtain some degree of separation between the reconstructed images along the optical axis direction, objects are usually recorded completely out of focus. Thus, the light scattered by the particles far away from the hologram plane is distributed over a very large area of the sensor, mixing with the background noise and the light diffracted by other particles. This fact limits the recording of large fluid regions, especially if the seeding is dense. The second drawback is the low system aperture, due to the narrow lobe of the light scattered by the particles in the forward direction and accentuated by the camera pixel size, which has a typical value of several micrometers. Thus, the reconstructed particle images size along the observation direction (its longitudinal size) is several times bigger than the real size, making difficult to determine accurately the particle position along the optical axis and reducing the spatial resolution. This circumstance is especially limiting for the regions furthest away from the sensor, where the defocusing and seeding density does not allow recording the particles clearly and completely. Despite these drawbacks, several authors (Gopalan et al. 2008, Talapatra et al. 2012, Toloui and Hong 2015, Lebon et al. 2016, Chen et al. 2017, Toloui et al. 2017) have shown that DIH is a feasible technique for studying very densely seeded flows in a large volume, sometimes at the cost of a cumbersome analysis, which often includes several iterations.

In this work we propose to apply DIH to measure the vortex breakdown bubble that appears near the cavity bottom at Re=2000. Thus, we recorded a 22x22x80mm^3 volume, being the longest dimension parallel to the camera optical axis. Working with such a large volume forced us to think about new analysis strategies to deal with the low spatial resolution along the optical axis in a flow with a high seeding density.

With this purpose, the holograms have been analyzed using a new method, called Adaptive Cross Correlation with Tracking From Beginning (ACCTFB), which includes the successful use of the reconstructed complex amplitude for particle localization under very unfavorable working conditions. Particle tracking is based on the three-dimensional cross-correlation of three-dimensional interrogation windows. The particularity of this hybrid method is that the working particle set defined in the first hologram is always used to find the particle position in every hologram in the series (Tracking From Beginning), what reduces the error in the particle location along its trajectory. This method provides an accurate 3D map of the velocity and spatial structure of the vortex-breakdown bubble and it is validated by the very good agreement of the measured velocity components with numerical data. A minimum of $1.8 \cdot 10^5$ particle positions and 5000 traces have been obtained by applying this method. A new criterion for determining the accuracy in the particle position along the optical axis, based on Particle Image Velocimetry concepts, has been introduced. The spatial resolution along the optical axis achieved in this case is 0.1 mm.

The cylindrical lid-driven cavity characteristics will be presented in Section 2. In Section 3, we will visualize the spatial structures formed in the cavity when applying Mach-Zehnder interferometry and PIV. These structures will be studied quantitatively in Section 4, by applying DIH to the measurement of the 3D-3C velocity field in a volume. The proposed new hologram analysis will be described in detail. In Section 5 the measured 3D-3C velocity field will be

shown. The experimental data are validated by the very good agreement of the measured velocity components with the numerical simulations.

2. Cylindrical cavity

The experimental set-up (Sancho et al. 2016) consists of a cylindrical cavity made of polymethyl methacrylate (PMMA) with an inner diameter (*2R*) of 8cm (figure 1). The aspect ratio of the cavity is set to $H/R = 2$, where H is the cavity height. Its top wall is rotating with an electronically controlled DC motor that operates at different angular velocities (ω). The motor works with angular velocities from 5 to 25 rad/s. In this way, the induced flow has Reynolds numbers $(Re=\omega R^2/\nu)$ from 1000 to 2300, always showing a laminar steady behavior.

In the experiments, a water-glycerin solution (60% v/v glycerin) has been used. Its kinematic viscosity (ν) changes between 10^{-5} and $1.25\text{x}10^{-5}$ m^2/s, within the range of room temperature of the experiments, and its density is $\rho \sim 1100$ kg/m^3. The flow has been seeded with Orgasol® spherical particles of 20μm in diameter. The solution and PMMA have similar refractive indices ($n_{solution}$ =1.42, and n_{PMMA} =1.49) so we are almost working in a refractive index matching condition. In order to avoid the image distortion that appears when an object is visualized through a curved surface, the cylinder was enclosed in a rectangular case ($14\text{x}14\text{x}14cm^3$) made as well of PMMA, and filled with the same water-glycerin solution.

Liquid with Orgasol® 20μm particles (in the particle trajectory visualization and DIH experiments) or with a different refractive index (in Mach-Zehnder interferometry) was introduced in the cavity through a bottom inlet (3mm of diameter) with a syringe pump (CHEMYX Fusion 100). The liquid was injected when the flow was in steady state at v=3.2mm/s. This velocity is 50 times smaller than the average velocity of the rotating top wall for Re=1000 and it does not affect significantly the velocity distribution imposed by the rotating wall.

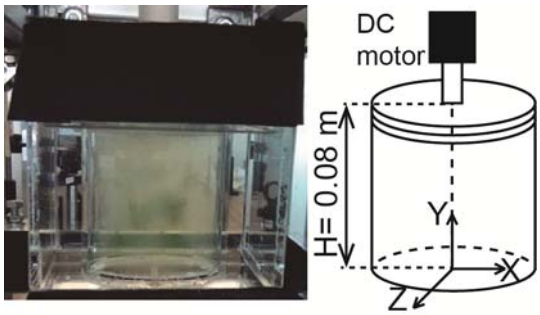

Figure 1: Photography and schematic drawing of the cylindrical cavity.

3. Visualization techniques

3.1. *Particle trajectory visualization*

The cavity central plane was illuminated with a high speed two-cavity New Wave Pegasus laser (λ = 527 nm, energy per pulse=10mJ at 1000 Hz), shaped into a sheet. A PCO camera (2560x2160 pixels, pixel size = 6.5μm, f/22, M=0.42) recorded the light scattered by the seeding particles. In order to allow for clear flow visualization, 50 images were recorded in one frame, setting the camera exposure time at 100 ms and the laser repetition rate at 2 ms (500 fps).

Figure 2 shows an image of the rotating flow (Re=1700) before injection (left) and immediately after the seeded liquid was injected through the bottom inlet.

These images show the secondary flow, superimposed to the main rotating flow, that has a three dimensional toroidal shape. The toroidal flow field can be distinguished due to the fast particles that enclose the vortex breakdown bubble. These fast particles form traces, while the slow particles are seen as bright dots inside the vortex breakdown bubble. In figure 2 (right), the stagnation point is clearly visible at the vortex breakdown bubble bottom.

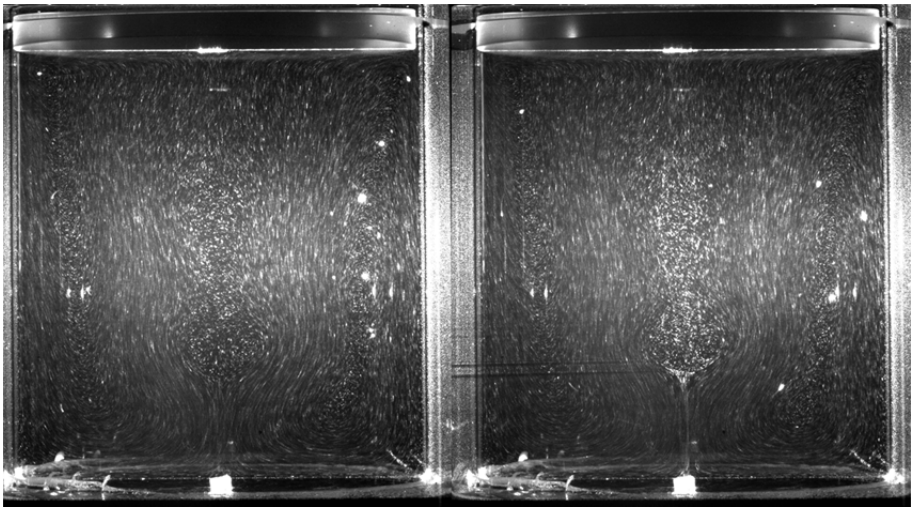

Figure 2. (Left) Rotating flow before injection; (right) additional seeded fluid is injected through the bottom inlet.

If highly seeded liquid is injected in the cavity it is possible to directly visualize the particle trajectories, i.e., the streamlines (Palero et al. 2016). Figure 3 shows a planar cut of the streamlines evolution, at Re=2000, as the injection took place. These images are obtained by adding ten frames, each one of them recorded with an exposure time of 100ms. The time interval between (a) and (b) is 2s, while between (b) and (c) is 1s. It can be seen that the injected liquid does not fill completely the inlet, but is going up through a thin line, which allows the streamline visualization. The spatial structure generated by the injected liquid is not axisymmetric because of small imperfections and misalignments of the rotating disk, as discussed in Sancho et al. 2016. Another interesting feature is the presence of two special zones with circular closed streamlines: a bright area in the cylindrical cavity center and two dark areas at both sides. The bright area is actually filled with particles, while the dark zones show the cross section of a particle empty toroid.

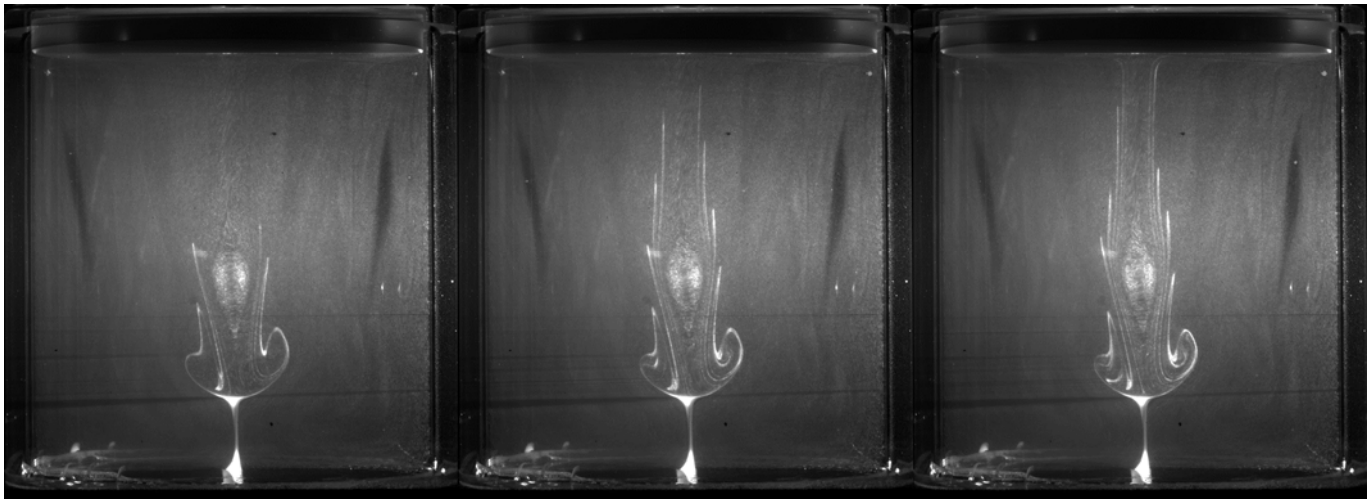

(a) (b) (c)

Figure 3: Streamlines visualization as the high seeded fluid is entering the cavity.

3.2. *Mach-Zehnder visualization*

Mach-Zehnder interferometry can be applied to visualize the mixing of fluids with different refractive index. Small changes in the refractive index can be measured by comparing the phase distributions of interferograms recorded at different times. These phase changes are directly related to the optical path length differences produced by refractive index changes along the beam path. In particular we can visualize the mixing temporal evolution when liquid is introduced in the swirling flow inside the cavity.

In this work we used an adapted Mach-Zehnder, whose set-up is shown in Figure 4. A lens formed the image of a plane in the digital sensor, where it interfered with a reference beam. In this way, we are recording a so-called image hologram. The reference beam is a divergent wave, whose origin was located at the same distance from the camera sensor than the lens aperture. Thus, we are also recording a lens-less Fourier hologram of the lens aperture plane as in a Digital Image Plane Holography (DIPH) configuration (Lobera et al. 2003, 2004). The selected plane was defined by a ground glass located in the case front wall. This ground glass is needed to visualize the phase changes in the cylindrical cavity. Information about changes in the liquid refractive index were obtained by comparing the phases of two object complex amplitudes reconstructed from holograms separated a certain time interval. Since these holograms have been recorded with a DIPH configuration, the object complex amplitude is reconstructed in the same way (Lobera et al. 2004).

In the experimental set-up the light from a solid state laser (λ= 532nm) was divided to form the reference and the object beams which were guided through optical fibers. The object beam was expanded with an optical system that allowed us to illuminate the whole cavity height. Its diameter was 130mm, its length, 160mm and its focal length, f'=500mm. A lens imaged the ground glass (f'=105mm, f/16, magnification, M=0.40) in a PCO camera (2560x2160 pixels, pixel size=6.5μm). The fluid in the cylindrical cavity was a water-glycerin solution ($n_{solution}$ =1.4295) and we changed slightly the refractive index of the injected liquid, by varying the proportion of water and glycerol (n=1.4256).

Series of 200 holograms were recorded at Re=2000 at 10 fps (time interval between two consecutive holograms ΔT=100 ms). The hologram recording was synchronized with the fluid injection. Figure 5 (a,b,c) shows the filtered phase difference maps

obtained by subtracting the phase maps obtained from two holograms separated a $t= 10*\Delta T$, while the liquid was being injected. That is, in figure 5a we can observe the phase difference obtained by subtracting the phase maps corresponding to the 10th and the 1st holograms; in figure 5b, we are subtracting the 50th and the 40th holograms' phase maps, and so on. These phase difference maps show how the injected liquid moves up following a helical path while mixing with the liquid inside the cavity. The vortex breakdown bubble is also visible. The process will end with both liquids completely mixed and a uniform refractive index within the cavity. This structure qualitatively agrees with the results obtained from the numerical simulation shown in figure 5d. In this way, we have been able to qualitatively describe the evolution of the mixing process and to reproduce the flow pattern reported in Sancho et al. 2016, without the use of the fluorescent liquid and avoiding adding Rhodamine to the tracer particles.

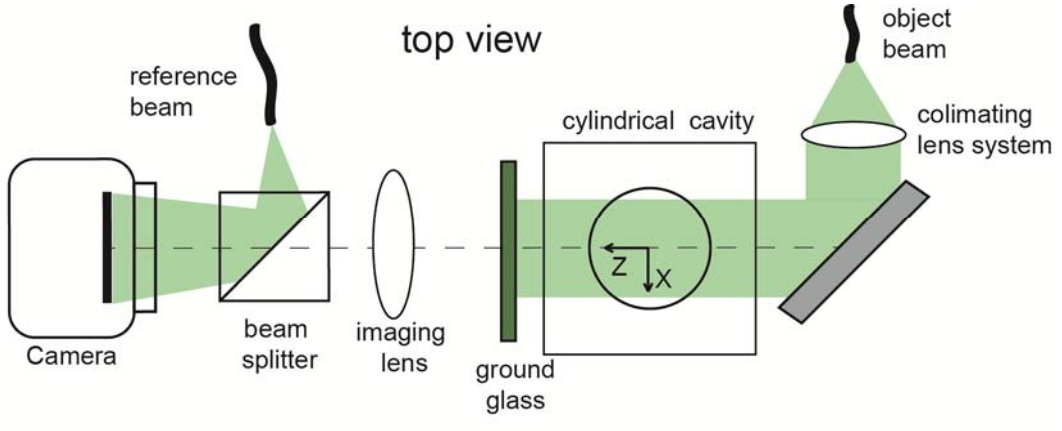

Figure 4: Adapted Mach-Zehnder set-up.

(a) (b) (c) (d)

Figure 5: Three dimensional mixing flow structure obtained from the phase difference maps by subtracting the phase maps corresponding to the holograms (a) 10-1; (b) 50-40; (c) 100-90. (d) Numerically predicted mixing iso-surface for Re = 2000.

4. Quantitative measurements

Digital in line holography has been applied for the quantitative measurement of the 3D-3C velocity field in a parallelepiped of 22x22x80 mm^3 which includes the vortex breakdown bubble formed near the cavity bottom. One of the most remarkable features is that the volume longest dimension is parallel to the optical axis (OZ). This implies that we will have to cope with the problems inherent to DIH already discussed in the introduction. The light scattered from particles far away from the hologram plane will be masked by the noise and the light scattered by other particles. Besides, the longitudinal size of the reconstructed particle image (d_l,) will be several times bigger than the real size, which reduces the spatial resolution in the optical axis direction. This parameter, d_l, defines the particle size as the voxels whose intensity is above 50% of the maximum intensity and it

is directly related with the numerical aperture (*NA*) and with the wavelength in the fluid ($\lambda_f = \lambda/n_{fluid}$). In our case, *NA* is mostly limited by the effective pixel size (*dx*) in the X and Y directions and d_l can be calculated as:

$$d_l = \frac{8d_x^2}{\lambda_f} \qquad (1)$$

4.1. Experimental set-up and hologram recording

A scheme of the experimental set-up is shown in figure 6. The fluid was illuminated with a collimated beam from a continuum laser (λ=532nm). The recorded volume was centered in the X axis and was 9mm over the cavity bottom. Holograms were recorded with a Photron SA2 camera (CMOS, 16 bits, 2048x2048 pixels, pixel size 10μm, 1000 fps). A lens formed the volume image in front of the camera sensor with magnification M=0.93. The distance between the camera sensor and the case front wall was 34cm. The distance from this wall to the cylinder axis was 7cm.

Liquid seeded with 20μm particles was injected during 10s with the system described in Section 2. Once the flow was stationary and just when the injection started, a series of 1000 holograms was recorded (at Re=2000) with a time interval between two consecutive holograms ΔT = 2ms.

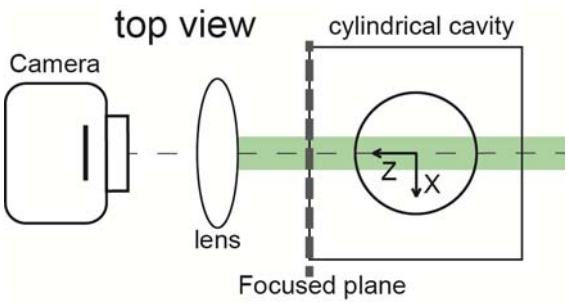

Figure 6: Digital In-line Holography set-up.

Introducing the lens in this set-up has several advantages. Its effect is equivalent to physically move the camera sensor to any plane in the light path. Besides, this plane will be in focus. This improves the hologram SNR while keeps the image of the seeding particles slightly defocused, which is essential to maximize the information recorded from each particle.

We chose to focus the case front wall (figure 6), i.e. the air/liquid interface, for two reasons: its Z-position is known and the object wave reconstruction will be done in only one medium. This allows us to reconstruct the holograms in the object domain just by dividing the wavelength by the fluid refractive index and the pixel size by the magnification. Focusing a plane inside the cavity implies that the hologram reconstruction has to be done in several steps due to the air/liquid interface. Alternatively, we can reconstruct the volume in the image domain, which requires a calibration for determining the Z-coordinate.

4.2 Hologram analysis

The hologram analysis includes the particle coordinate determination and its tracking along a series of holograms by means of a new method, called Adaptive Cross-Correlation Tracking From Beginning. The complete analysis is represented schematically in figures 7 and 8.

First, the hologram SNR is enhanced. The direct inspection of the flow shows that the different refractive index of the injected liquid produces a shadowed area in the holograms. This structure changes during the recording time, which prevents us from using the whole series to compute the average hologram. The moving average is calculated for each hologram, taking the ten previous holograms and the next ten. The enhanced hologram is obtained after subtracting the moving average and normalizing its intensity (figure7).

Coarse particle coordinate estimation. The complex amplitude distribution of the object wave is reconstructed at different Z-planes *(Δz=2mm*) by applying the Convolution Method (Schnars and Jüptner 2005). This relatively coarse sampling is forced by the value d_l (defined by eq. 1) but has the additional advantage of reducing the computational cost and memory requirements. In our case, $dx=dy$ =10μm, λ_f =373nm, and thus, d_l=2.14mm.

The reconstructed volume is divided into equally sized parallelepipeds (our 3D interrogation window, 3DIW) where the maximum global intensity is calculated. We chose a 3DIW whose dimensions were 40x40x40 pixel^3, which corresponds to 0.43x0.43x80 mm^3, extending over the cavity whole length. Pixels in the XY plane are defined by the sensor pixel size and by the magnification. In the Z direction, we will define the pixel as the sampling interval, i.e. pixel_z=2 mm, in this step. In order to optimize the volume sampling, the 3DIW were overlapped a 50% in the XY plane, providing around 10000 preliminary particles in the first hologram.

Handling such a high quantity of data makes the analysis cumbersome and is unnecessary as half of the maximum are spurious peaks or just oversampling due to the 3DIW overlapping. The duplicated particles are removed and the remaining ones are ordered by decreasing intensity. As the particle intensity decreases with the distance to the hologram plane, most of the detected particles in the cavity are close to the camera sensor. Special care is taken in choosing a working particle set where the particles are homogenously distributed along the optical axis direction. Only one thousand particles, but uniformly distributed, are kept, giving a particle density of 0.0002 ppp in an 80 mm long volume.

Fine particle coordinate estimation. In order to accurately locate each particle, its image extension has to be known. An adaptive threshold is introduced as the particle image varies with its axial position. First, a smaller 3DIW (10x10x30 pixel^3, pixel_z=0.2 mm) is considered. The particle will be defined by the voxels whose intensity adds up the 64% of the total intensity in this 3DIW. In particles near the focused plane, this percentage can be achieved with as few as three voxels, whereas particles farther from the sensor could need even thirty voxels. The filter is automatic and it has shown a great robustness.

Once the particle image is defined, its transversal (X, Y) coordinates are given by the centroid of the intensity distribution. The centroid calculation is not used for the axial coordinate measurement, due to the poorer resolution in this dimension inherent to the inline configuration. Instead, a polynomial fit is carried out and the maximum is selected as the particle Z coordinate. The particle is kept in the working set only if the new coordinates are close enough to the global maximum calculated previously, being the maximum shift allowed (Δx<0.025mm, Δy<0.025mm, Δz<3mm). Particles will be analyzed in decreasing order of intensity and will be eliminated from the reconstructed image before looking for the next one. Once the process is completed, the final particle set consists of roughly 500 particles.

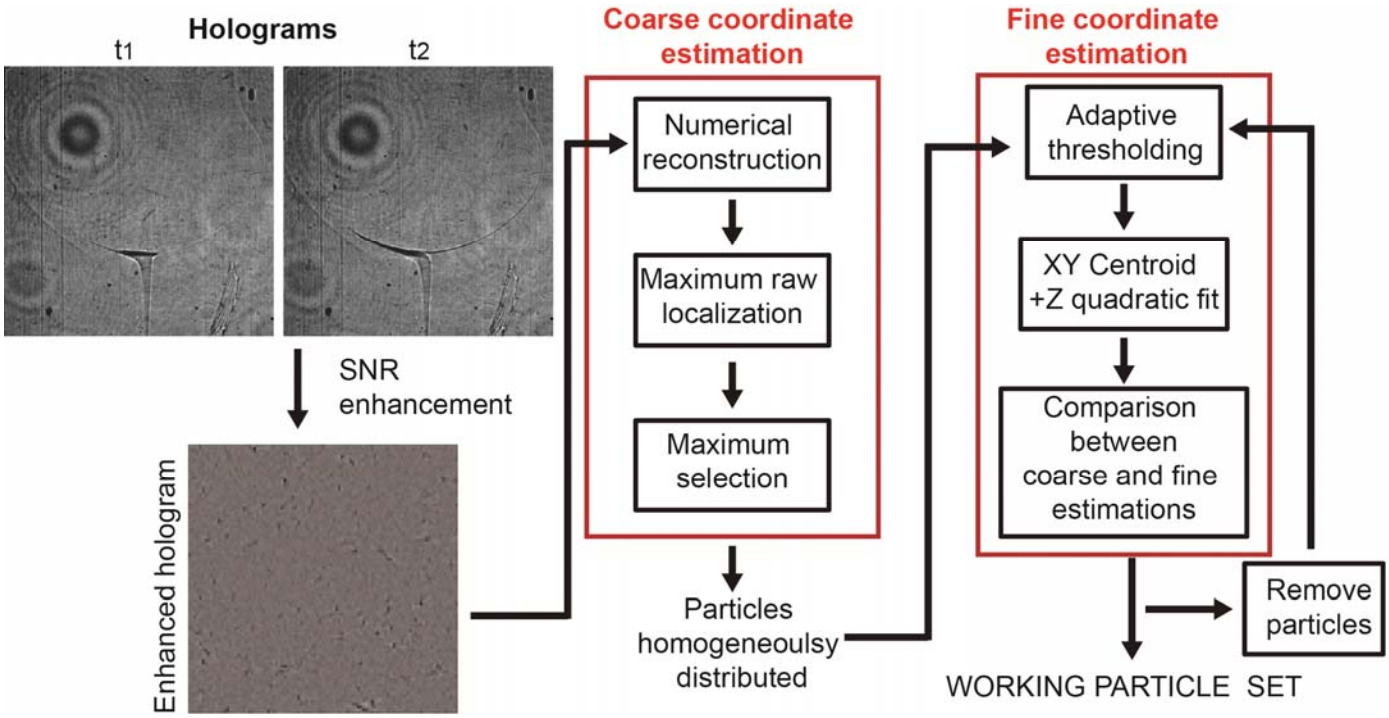

Figure 7: Procedure to find in the first hologram the particle working set which will be tracked in the hologram series.

Adaptive Cross-Correlation Tracking From Beginning (ACCTFB)

The set of particles found in the first hologram is tracked in a multi-pass, adaptive interrogation process. This adaptive method is based on the 3D cross-correlation of 3D interrogation windows, in a similar approach to the one used in PIV. First, the particle displacement between the first and second holograms has to be calculated. The Tracking From Beginning idea is introduced for determining the particle trajectory along whole hologram series.

Particle displacement between the first and second holograms is obtained in several steps in order to maximize the accuracy of the measurement. The process starts by calculating the intensity 3D cross-correlation of two 3DIW (32x32x15 pixel^3, pixel_z=0.2 mm) centered in the particle location obtained from the first hologram. The displacements in the cavity with this *Re* are expected to be within the measured range allowed by these 3DIW. The correlation peak might be deformed due to the contribution of out-of-focus particles in the reconstructed volumes. To improve the SNR a Gaussian filter, centered in the correlation peak, is applied in the 3DIW of the second hologram and a new correlation is calculated.

This second 3D correlation allows us to define the correlation peak as the voxels whose intensity adds up the 64% of the total intensity. It is the same adaptive, automatic and robust criteria used previously. The transversal particle displacement $(\Delta x_2, \Delta y_2)$ is obtained from the correlation peak centroid. From this displacement the particle velocity components are calculated ($Vx_2=\Delta x_2/\Delta T$; $Vy_2=\Delta y_2/\Delta T$). The particle position in the second hologram (x_2, y_2) is obtained by adding to the displacements the particle coordinates in the first hologram (see figure 8).

The Z displacement (Δz_2) resolution is improved by computing a third cross-correlation, which uses the complex amplitude instead of the intensity. Wormald and Coupland (2009), demonstrated that the complex amplitude cross-correlation provides a

sharper correlation peak than the intensity cross-correlation, due to the fact that the complex amplitude correlation is an entirely linear process, which compensates the phase aberrations introduced by the imaging system.

So far, the complex amplitude cross-correlation has been hindered by its high sensitivity to the noise coming from the out-of-focus particles. This noise can generate a secondary peak in the correlation which masks the real displacement peak, especially when the out-of-focus particles share a similar movement (Coupland et al. 2000). As the transversal particle coordinates are well defined, we can reduce the 3DIW size to the particle size (8x8x15 pixel^3; pixel_z= 0.2mm). In this way, the reconstructed particle images are not affected by the coherent noise coming from the out-of-focus particles that forced the use of the intensity correlation in the previous steps. The complex amplitude cross-correlation is one of the keys of the ACCTFB method good performance.

There is not a general consensus on how to define the spatial resolution in the optical axis direction. Here, we propose to extrapolate some PIV concepts related with the accuracy in the velocity measurement. In PIV the in-plane velocity components are obtained from 2D cross-correlations between 2D interrogation windows. Then, it is assumed that the correlation peak position can be calculated with sub-pixel accuracy by using a three-point estimator (Raffel et al. 1998-2007). This estimator is usually a Gaussian or a polynomial (parabolic) fit that works best for narrow correlation peaks obtained when the particle image diameter is 3 pixels. In such a case, the accuracy in the measured displacement can be taken as one tenth of the pixel size. In our case as dx =10μm, our spatial resolution will be 1μm.

Since we have calculated the particle displacement with the 3D cross-correlation between 3D interrogation windows selected in two holograms, we can apply the same reasoning to estimate ΔZ and its accuracy. We can use a three-point estimator to obtain the position of the correlation peak with sub-pixel accuracy. However, in the holographic reconstruction the sampling along the optical axis, which we will call the 'longitudinal pixel size' (*lps*), is user defined. In order to apply the three-point estimator, we need to establish a *lps* large enough to ensure that the particle is defined with 2-3 'pixels'. Two criteria can be used to set the *lps* value. One is the theoretical particle longitudinal size given by d_l. The second comes from the direct inspection of the reconstructed particle images, whose mean size is d_m. This parameter is calculated with the points in the particle image whose intensity is above the 50% of the maximum intensity. In the present case, d_l =2.14mm and d_m=3mm±1mm (obtained from 500 reconstructed particles). Thus, it seems reasonable to define *lps*=1mm. As the particle image covers 3 pixels, we can assume that the particle displacement is being measured with subpixel accuracy (one tenth of the pixel size), i.e., 0.1 mm. This value gives us the spatial resolution along the optical axis (Z) direction, which can be considered a very good value.

Once the three coordinates are found in the second hologram, the particle must be tracked along the hologram series. This can be done by calculating the 3D cross-correlation between reconstructed 3DIW in consecutive holograms, at the cost of an accumulative error in the particle position. Ideally, the highest accuracy in the displacement measurement would be achieved correlating the first hologram with every hologram in the series. This is not reasonable because the 3DIW size should be increased as the particle is moving. The only way for applying the Tracking From Beginning is to calculate the 3D cross-correlation between one 3DIW in the first hologram, centered in the particle, and a shifted 3DIW in the Nth hologram, but centered in the particle position obtained from the (N-1)th hologram. Thus, we can maintain the same 3DIW size as if the cross-correlation were performed between consecutive holograms. In our case, this size is 32x32x15 pixel^3 (pixel_z=0.2 mm). We will

obtain in that way (Δx_N, Δy_N). The complex amplitude cross-correlation of 8x8x15 pixel^3 (pixel_z = 0.2 mm) 3DIW will provide Δz_N. This TFB method allows us to follow the particle trajectory along one hundred holograms.

It is not possible to follow the particles along the whole hologram series, since we are not observing the whole cavity volume. New particles have to be included in the working set to replace those that are leaving the recorded volume. Restarting the analysis every one hundred holograms has proved to be enough to have a complete flow description. This means that around 500 particles are followed along 100 holograms. Then, a new working set of particles is found again and the whole procedure, including the Tracking from Beginning, is repeated. Wrong displacements are found mostly in the vortex breakdown bubble due to the shadows produced by the fluctuations in the liquid refractive index. Those measurements are eliminated by means of a polynomial fit. The measured points are further reduced by the particles that leave the field of view. As a result we end up with a final number of $1.8 \cdot 10^5$ measured points. Each measurement point includes the 3D particle position and the three velocity components.

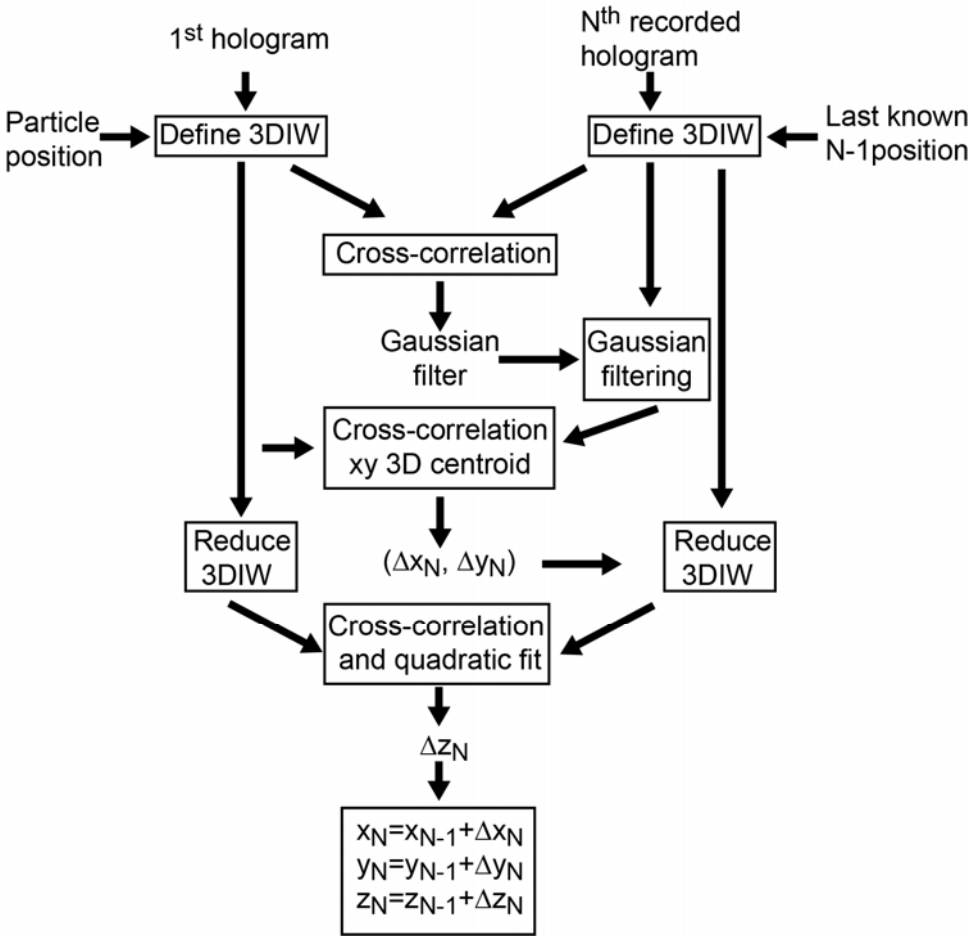

Figure 8: Block diagram of the Adaptive Cross-Correlation Tracking From Beginning method.

Figure 9 compares the performance of the TFB method against an approach where the particle trace is obtained by calculating the displacement between consecutive holograms. One hundred holograms were analyzed with both methods. Figure 9a shows the particle position and the spatial distribution of *Vx* obtained with the TFB while figure 9b shows the results obtained with the standard procedure. Even with only one hundred holograms some of the most important flow features can be distinguished when the TFB method is applied. In figure 9a we can appreciate the fluid rotation and its axial symmetry. The vortex breakdown bubble can be also faintly distinguished in the center of the measured volume (points that are rotating at a low speed or that are

not rotating at all). However, the standard procedure (figure 9b) fails completely in following the particle in its movement in the volume analyzed, reproducing an inaccurate/wrong particle trace and a wrong velocity measurement.

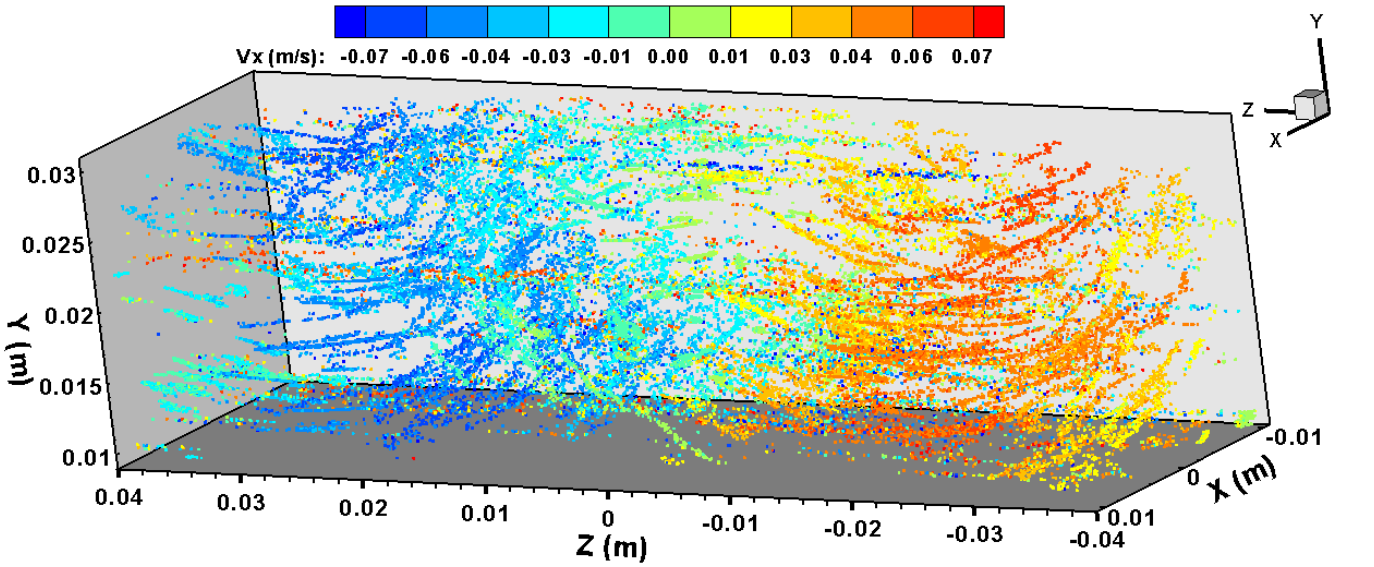

(a)

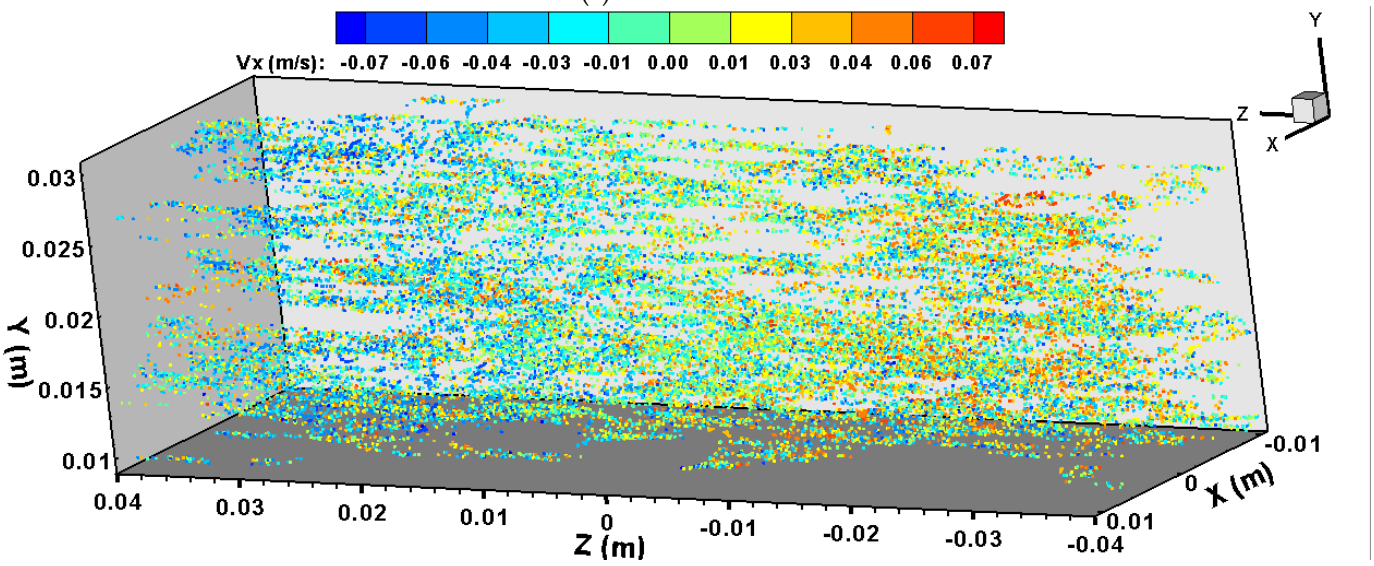

(b)

Figure 9. Particle traces obtained from the analysis of 100 holograms: a) with the TFB algorithm; b) without the TFB algorithm.

4.3 Experimental results

The DIH measured volume at Re=2000 is shown in figure 10. At this Re number a vortex breakdown appears at the axis of the cavity at 0.016m<Y<0.040m (see for example Fig. 5.f of Sancho et al. 2016). Part of this zone can be seen in figure 10 and the effect of the vortex breakdown in the three components of the velocity vector is shown. Let us point out that we are displaying the particles traces along the Z axis, which corresponds to the optical axis, where the spatial resolution and accuracy are smaller.

In the center of the *Vx* field the vortex breakdown bubble is clearly visible, although few particles were tracked in that region. There, the particle displacement is very small and cannot be measured accurately. As it can be observed, when the vortex breakdown occurs, the velocity at the center of the cavity decreases. We can also visualize the secondary flow, with a three dimensional toroidal shape, superimposed to the main rotating flow. This can be seen in a top view of the *Vy* distribution. Here

the axial symmetry is perfectly noticeable. The third velocity component, Vz is equivalent to Vx due to the rotational symmetry. In fact, Vz should have the same values as Vx in -0.011<Z<0.011m, i.e. -0.04<Vz<0.04m/s. In spite of the low spatial resolution and accuracy (100μm for Δz vs 1 μm for Δx and Δy), the Z coordinate and Vz have been accurately measured as the particle traces are correctly located and the Vx and Vy agree with the numerical simulations.

In order to validate the measured data, the normalized velocity components are compared with the numerical simulations (Sancho et al. 2016). The velocity was normalized with ωR, while the coordinates Y* and Z* correspond to Y, Z, divided by H and R respectively. Figure 11 shows the velocity profiles of the axial velocity component Vy* and the radial component Vx* along the optical axis (Z*), at two heights Y*= 0.12 and Y*= 0.38, corresponding to a line close to the reactor bottom (Y = 9 mm) and to the upper part of the recorded volume (Y = 31 mm). Particles ascend the cavity axis and descend as they approach to the walls. Good measurements are obtained close to the cavity wall, where the particle velocity is zero. It can be seen that the experimental velocities (Vy*) next to the cylindrical wall, at Z* = 0.9 and Z* = -0.9, are not perfectly axisymmetric. Some fluctuations appear in the measured data due to imprecision in the Z-coordinate rather than in the velocity. In conclusion, we can assure than the experimental velocity profiles are in good agreement with the numerical profiles.

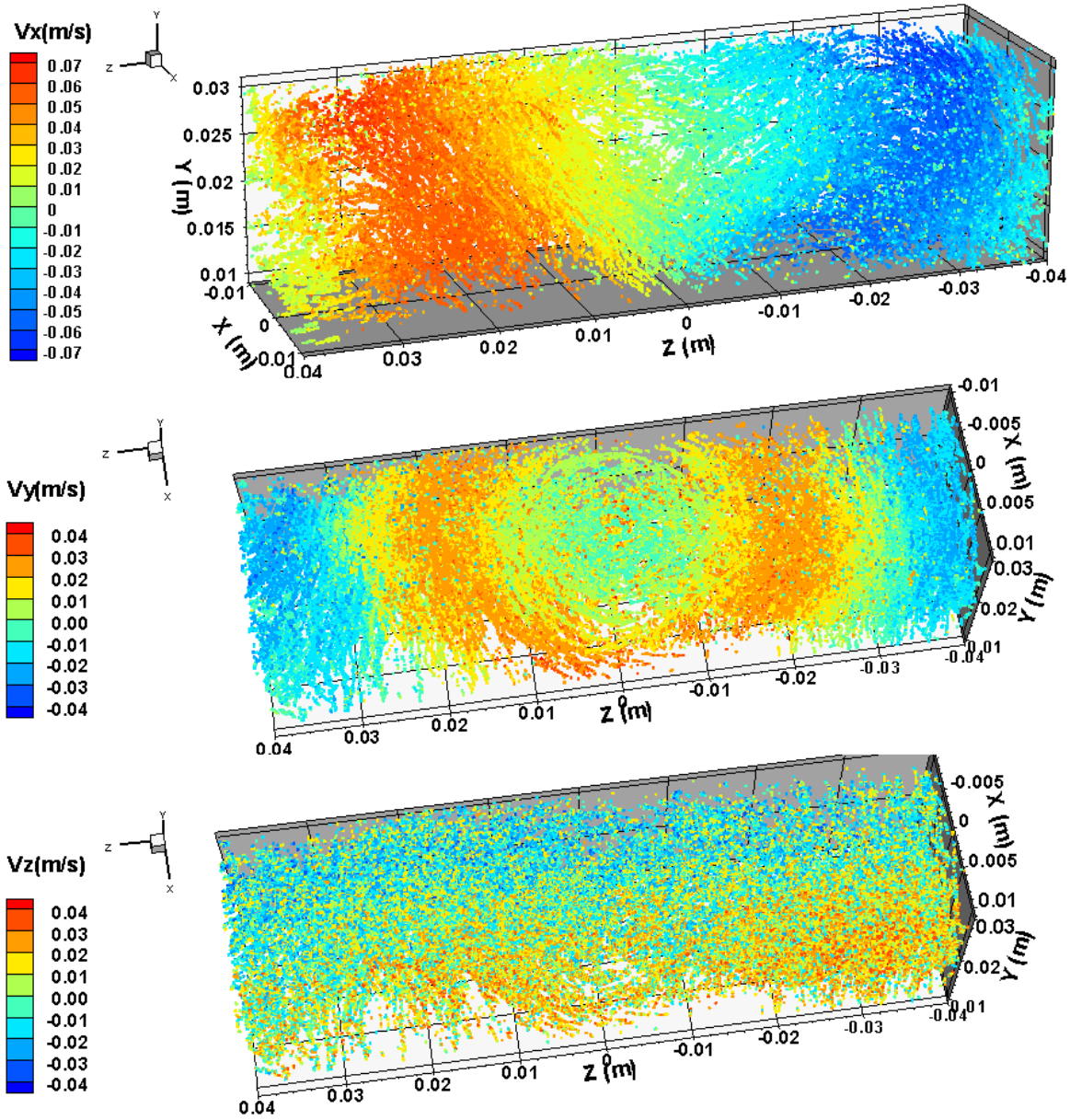

Figure 10. 3D representation of the particle position and (Vx, Vy, Vz) for the whole recorded volume

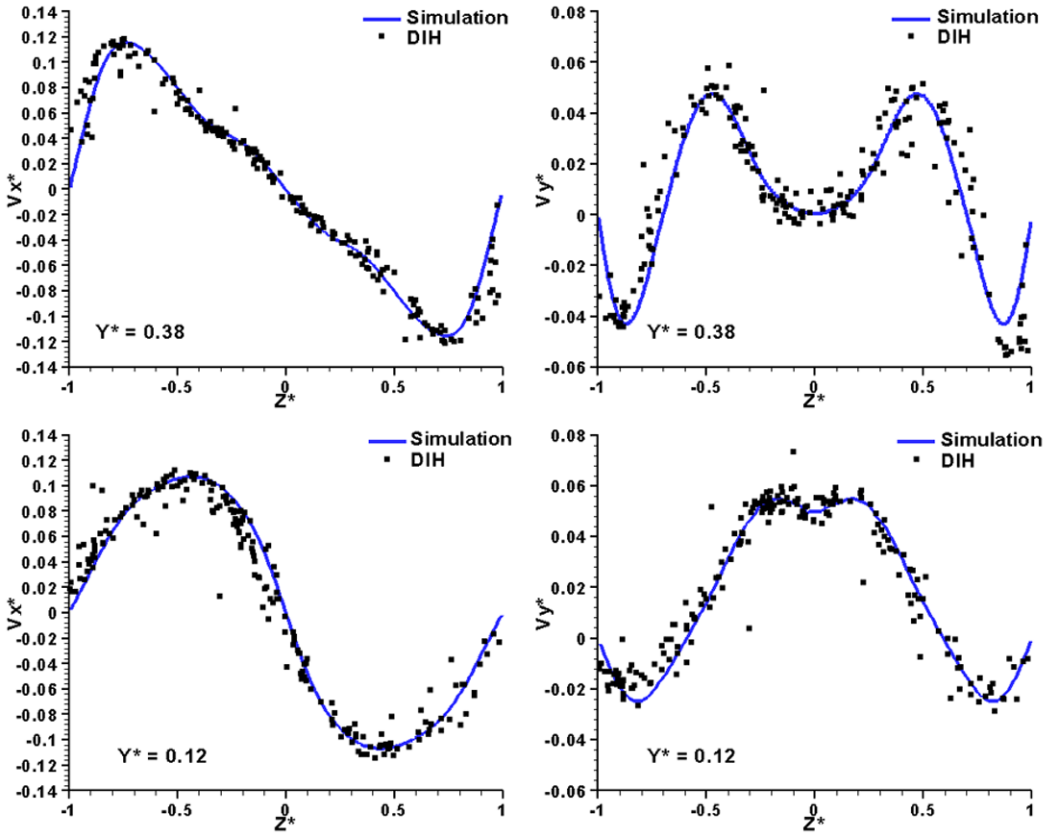

Figure 11: Comparison of the measured and simulated Vx* and Vy* for different heights in the cylindrical cavity.

5. Conclusions

It has been shown that it is possible to obtain qualitative information of the three-dimensional flow features in a lid-driven cylindrical cavity by applying optical, non-intrusive techniques as the Mach-Zehnder interferometry or PIV. With an adapted Mach-Zehnder interferometry set-up we have been able to visualize the mixing of the injected liquid within the swirling flow inside the cavity, by the analysis of the changes in the refractive index in the mixing process. With PIV, and injecting a highly seeded liquid, we have been able to visualize the flow streamlines.

The 3D-3C velocity field has been accurately measured in a volume of 22x22x80mm^3 inside a highly seeded flow, which includes the vortex breakdown bubble, by applying Digital In line Holography (DIH). A new method, called Adaptive Cross-Correlation Tracking From Beginning (ACCTFB), has been introduced. This method is based on the three-dimensional cross-correlation of three-dimensional interrogation windows in a similar approach to the one used in PIV to obtain the two-dimensional velocity field. The complex amplitude for particle localization in a flow with high seeding density has been successfully used.

Each particle was tracked along one hundred holograms, using always the particle position in the first hologram (Tracking Form Beginning), therefore avoiding the accumulative error that appears when consecutive recordings are used to follow the particle. The analysis based on the cross-correlation of interrogation windows, allows introducing a new criterion for the estimation of the accuracy in the measurement of the particle Z displacement and, therefore, in the particle Z position. This criterion is based on PIV concepts. We have found that the spatial resolution in the optical axis direction achieved in this case is 0.1 mm. A minimum

of $1.8 \cdot 10^5$ particles positions and 5000 traces has been obtained by applying this method. The measured velocity field was compared with the numerical simulation, showing very good agreement. Although it has been proven in a stationary flow, this tracking method can be also applied to the study of 3D turbulent flows.

6. Acknowledgments

Authors thank the Spanish Ministerio de Economía y Competitividad (MINECO) and European Commission FEDER program (project DPI2016-75791-C2-2-P/1-P) and Gobierno de Aragón- Feder 2014-2020 "Construyendo Europa desde Aragon". (Laser Optical Technology - E44_17R- research group) for financial support.

7. References

Arroyo MP, Hinsch KD (2008) Recent developments of PIV towards 3D measurements. Particle Image Velocimetry: New Developments and Recent Applications. Ed. A Schroder, CE Willert, Springer, New York, pp. 127–54.

Brøns M, Shen WZ, Sørensen JN, Zhu WJ, (2007) The influence of imperfections on the flow structure of steady vortex breakdown bubbles, J. Fluid Mech; 578: 453–466.

Brown GL, Lopez JM. (1990) Axisymmetric vortex breakdown Part 2. Physical mechanisms, J. Fluid Mech.; 221: 553–576.

Cabeza C, Sarasúa G, Martí AC, Bove I, Varela S, Usera G, Vernet A. (2010) Influence of coaxial cylinders on the vortex breakdown in a closed flow, Eur. J. Mech. B. Fluids.; 29 (3) 201–207.

Chen Y, Guildenbecher DR, Hoffmeister KNG, Cooper MA, Stauffacher H L, Oliver MS, Washburn EB. (2017) Study of aluminum particle combustion in solid propellant plumes using digital in-line holography and imaging pyrometry, Combustion and Flame; 182: 225–237

Coupland J M, Lobera-Salazar J, Halliwell N A (2000) Fundamental limitations to the spatial resolution and flow volume that can be mapped using holographic particle image velocimetry, Proc. SPIE 4076, Optical Diagnostics for Industrial Applications, doi: 10.1117/12.397966.

Elsinga GE, Scarano F, Wieneke B, van Oudheusden BW. (2006) Tomographic particle image velocimetry. Experiments in Fluids; 4:933–947

Escudier MP. (1984) Observations of the flow produced in a cylindrical container by a rotating endwall, Experiments in Fluids; 2 (4); 189–196.

Gelfgat AY, Bar-Yoseph PZ, Solan A. (1996) Stability of confined swirling flow with and without vortex breakdown, J. Fluid Mech.; 311: 1–36.

Gopalan B, Malkiel E, Katz J. (2008). Experimental investigation of turbulent diffusion of slightly buoyant droplets in locally isotropic turbulence. Physics of Fluids, 20(9), 095102.

Katz J, Sheng J. (2010) Applications of Holography in Fluid Mechanics and Particle Dynamics, Rev. Fluid Mech.; 42:531-555.

Lebon B, Perret G, Coëtmellec S, Godard G, Gréhan G, Lebrun D, Brossard J. (2016) A digital holography set‑up for 3D vortex flow dynamics, Experiments in Fluids; 57:103 DOI 10.1007/s00348-016-2187-8

Lobera J, Andrés N, Arroyo MP. (2003) Digital Image Plane Holography as a three-dimensional flow velocimetry technique, SPIE 4933; 279-284

Lobera J, Andrés N, Arroyo MP (2004) Digital speckle pattern interferometry as a holographic velocimetry technique. Meas Sci Technol 15:718–724

Lopez JM. (1990) Axisymmetric vortex breakdown Part 1. Confined swirling flow, J. Fluid Mech; 221: 533–552.

Lopez JM, Perry AD. (1992) Axisymmetric vortex breakdown. Part 3 Onset of periodic flow and chaotic advection, J. Fluid Mech.; 234: 449–471.

Lucca-Negro O, O'Doherty T. (2001) Vortex breakdown: a review, Prog. Energy Combust. Sci.; 27 (4) 431–481.

Palero V, Lobera J, Arroyo MP. (2010) Three-component velocity field measurement in confined liquid flows with high speed digital image plane holography. Experiments in Fluids, 49:471-483.

Palero V, Lobera J, Brunet P, Andrés N, Arroyo MP. (2013) 3D characterization of the inner flow in an oscillating drop Experiments in Fluids. 54:1568 DOI 10.1007/s00348-013-1568-5

Palero V, Andrés N, Arroyo M P, Sancho I, Vernet A, Pallares J. (2016) Numerical and experimental study of mixing in a small-scale model reactor. 18th International Symposium on Applications of Laser Techniques to Fluid Mechanics, Lisbon, Portugal.

Pan G, Meng H. (2003) Digital holography for particle fields: reconstruction by use of complex amplitude. Appl Opt; 42:827–833

Raffel M, Willert C, Wereley S, Kompenhans J. Particle Image Velocimetry, a practical guide, Springer Verlag. 1998-2007

Sancho I, Varela S, Vernet A, Pallares J. (2016) Characterization of the reacting laminar flow in a cylindrical cavity with a rotating endwall using numerical simulations and a combined PIV/PLIF technique. International Journal of Heat and Mass Transfer. 93: 155-166.

Schnars U, Jüptner WPO (2005) Digital holography. Springer, Berlin

Shankar PN, Deshpande MD (2000) Fluid mechanics in the driven cavity. Annual Review of Fluid Mechanics; 32(1); 93-136

Sheng J, Malkiel E, Katz J. (2003) Single beam two-views holographic particle image velocimetry. Appl Opt.; 42:235–250

Sørensen JN, Naumov I, Mikkelsen R. (2006) Experimental investigation of three-dimensional flow instabilities in a rotating lid-driven cavity. Experiments in Fluids; 41(3), 425-440.

Sotiropoulos F, Ventikos Y. (2001) The three-dimensional structure of confined swirling flows with vortex breakdown, J. Fluid Mech.; 426: 155–175.

Spohn A, Mory M, Hopfinger EJ. (1998) Experiments on vortex breakdown in a confined flow generated by a rotating disc, J. Fluid Mech.; 370: 73–99.

Talapatra S, Sullivan J, Katz J, Twardowski M, Czerski H, Donaghay P, Hong J, Jan R, McFarland M, Nayak A, Zhang Cao (2012). Application of in-situ digital holography in the study of particles, organisms and bubbles within their natural environment. In Ocean Sensing and Monitoring IV (Vol. 8372, p. 837205). International Society for Optics and Photonics.

Toloui M, Hong J (2015). High fidelity digital inline holographic method for 3D flow measurements. Optics Express, 23(21), 27159-27173.

Toloui M, Mallery K and Hong J (2017) Improvements on digital inline holographic PTV for 3D wall-bounded turbulent flow measurements. Measurement Science and Technology; 28 044009 (15pp) doi:10.1088/1361-6501/aa5c4d

Vest CM. Holographic interferometry, Wiley Series in Pure and Applied Optics. Wiley, New York 1979

Wormald SA, Coupland J. (2009) Particle image identification and correlation analysis in microscopic holographic particle image velocimetry, Appl. Opt. 48, 6400-6407